JOURNAL OF MATERIALS SCIENCE **34** (1999) 407–416

Microstructural development in cast and aged Ni–Al–Cr-based alloys derived from the B2 type β-NiAl structure

W. F. GALE, Z. A. M. ABDO, R. V. NEMANI
Auburn University, Materials Research and Education Center, 201 Ross Hall, Auburn, AL 36849, USA

The formation of intermetallic compounds consisting of nickel-rich B2-type NiAl (β-phase) ductilized by two-phase A1 (γ)/$L1_2$ (γ') regions provides the possibility of combining ductility and high-temperature performance. Similar microstructures can also form the basis of high-temperature shape memory alloys, due to martensitic transformation of the β-phase to an $L1_0$-type product. One route by which $\beta-\gamma/\gamma'$ microstructures can be produced involves the use of chromium as a γ-stabilizer. However, microstructural development in such a case is complicated by the formation of α-Cr precipitates.

This paper examines microstructural development and stability in cast Ni–25 at % Al–14 at % Cr, Ni–29 at % Al–22 at % Cr and Ni–27 at % Al–8 at % Cr alloys, together with a more complex material, namely, Ni–20 at % Al–13 at % Co–9 at % Cr–4 at % Ti–1 at % Mo–1 at % V. Both the as-cast condition and samples aged at 850 and 1100 °C for 140 h are examined using transmission electron microscopy. The paper discusses the formation of $L1_0$ martensite, intradendritic γ', interdendritic γ/γ' and α-Cr precipitation.

1. Introduction

There has been considerable interest in recent years in the ductilization of materials derived from the B2 compound NiAl (commonly denoted as the "β" phase) by the addition of various second phases [1–7]. A significant body of this work has employed the γ' ($L1_2$-type compound with a nominal composition of Ni_3Al) and γ (Al-type nickel-base solid solution) phases. Microstructures based on β-γ, β-γ', and β-γ/γ' have been examined in various investigations, [2, 3, 5, 7] and considerable scope for ductilization exists. Of these materials, the β-γ/γ' alloys are particularly interesting, as these would seem to offer the possibility of combining low-temperature ductility with high-temperature creep resistance. β-γ/γ' alloys can also form the basis of high-temperature shape-memory alloys. In the β-γ/γ' materials, the shape-memory effect is associated with the formation of thermoelastic $L1_0$-type martensite from nickel-rich β [8], while the presence of the γ/γ' regions reduces the risk of brittle fracture at low temperatures.

Much of the work conducted to date on β-γ/γ' microstructures has focused on iron-bearing alloys. Iron stabilizes the γ-phase (particularly at the expense of γ' [9]) and allows the formation of β-γ/γ' rather than β-γ' [5–7]. Typically, the addition of iron produces β-γ/γ' microstructures in low aluminum alloys such as Ni–20 at % Al–30 at % Fe. In contrast, one of the authors has previously found that the use of chromium as a γ-stabilizer allows the formation of β-γ/γ' microstructures in relatively aluminum-rich materials such as cast Ni–24 at % Al–21 at % Cr [10, 11]. A further increase in the aluminum content of these materials would be attractive from the standpoint of increased environmental resistance and reduced density. Hence, the present investigation examines microstructural development in three relatively aluminum-rich arc-melted alloys: Ni–25 at % Al–14 at % Cr, Ni–29 at % Al–22 at % Cr and Ni–27 at % Al–8 at % Cr. These alloys were selected to offer a range of (γ-stabilizing) chromium to (γ'-forming) aluminum ratios in materials with higher aluminum contents than investigated previously.

In a previous work by one of the authors [12], the occurrence of highly stable β-γ/γ' microstructures was observed in a complex multi-element cast alloy originally produced to simulate phase transformations in aluminide diffusion coatings. The original material contained over 1 at % C, which resulted in the extensive formation of $M_{23}X_6$ precipitates (for which M was mostly chromium and X carbon). Thus, the formation of $M_{23}X_6$ served to tie up γ-stabilizing chromium. In the present investigation, microstructural development is examined in a cast alloy: Ni–20 at % Al–13 at % Co–9 at % Cr–4 at % Ti–1 at % Mo–1 at % V, which is similar to that examined previously, but from which carbon has been removed.

2. Experimental procedures

Arc-melted samples of Ni–25 at % Al–14 at % Cr, Ni–29 at % Al–22 at % Cr, Ni–27 at % Al–8 at % Cr and

0022–2461

Ni–20 at % Al–13 at % Co–9 at % Cr–4 at % Ti–1 at % Mo–1 at % V were produced in the form of 30 g buttons. These buttons were each inverted and arc-melted six times to promote mixing. Homogenization treatments were conducted in an argon atmosphere at temperatures of 850 and 1100 °C for 140 h, followed by furnace cooling to room-temperature.

Transmission electron microscopy (TEM) specimens were prepared from each of the arc-melted alloys in the as-cast condition and after homogenization at 850 and 1100 °C. Ion milling, rather than electropolishing, was employed to manufacture the TEM specimens, as severe problems with differential polishing have been experienced previously by the authors with alloys of this type. Argon ion milling was conducted using a Gatan DuoMill employing an accelerating voltage of 5 kV with dual guns operated at a current of 500 μA per gun and with gun–specimen angles of 13°. The TEM investigations were supplemented by light and scanning electron microscopy (LM and SEM, respectively). SEM and LM studies were conducted on metallographic samples electroetched at 3 V in a solution consisting of 70 vol % distilled water, 10 vol % glycerol, 15 vol % hydrochloric acid and 5 vol % nitric acid. For analytical investigations, some SEM work on polished, but unetched, samples was also conducted.

TEM investigations used a JEOL JEM 2010 instrument operated at 200 kV. Throughout this paper, the following nomenclature is employed: "BF" and "DF" indicate bright field and dark field micrographs, respectively, "**B**" represents the beam direction for selected area diffraction (SAD) and nano-beam diffraction (NBD) patterns and "**g**" indicates the reciprocal lattice vector of the operating reflection in DF images. SEM studies employed a JEOL JSM 840 instrument operated at 20 kV. In this paper, "SEI" represents a SEM-derived secondary electron image. Analytical studies were conducted using energy dispersive X-ray spectroscopy (EDS) via ultra-thin window (UTW) detectors and Link Systems Isis analyzers attached to the JEM 2010 and JSM 840 instruments. Quantitative SEM-based and qualitative TEM-based analyses were performed.

3. Results and discussion

In this section, microstructural development in the Ni–25 at % Al–14 at % Cr, Ni–29 at % Al–22 at % Cr, Ni–27 at % Al–8 at % Cr and Ni–20 at % Al–13 at % Co–9 at % Cr–4 at % Ti–1 at % Mo–1 at % V materials examined in the present work will be discussed. The general microstructural and compositional features of these materials will first be described and specific phase transformations will then be considered. The overall microstructural and compositional features of the four alloys examined in this work are contained in Tables I and II, respectively.

TABLE I Summary of the key microstructural features of the materials examined

Material (at %)	Condition	Dendrite matrix	Purely intradendritic second phases	Interdendritic matrix	Purely interdendritic second phases	Precipitates crossing dendrite boundaries
Ni–25 Al–14 Cr	As-cast	Martensitic	α-Cr spheres	Mostly γ'	α-Cr needles	α-Cr needles
	850 °C aged	β	α-Cr spheres	γ'	α-Cr needles	α-Cr needles
	1100 °C aged	β	γ' and α-Cr	γ/γ'	None	None
Ni–29 Al–22 Cr	As-cast	Martensitic	α-Cr spheres	γ/γ'	None	α-Cr needles
	850 °C aged	Mostly β	γ' ellipsoids	γ'	α-Cr needles	None
	1100 °C aged	β	None	γ'	None	α-Cr needles
Ni–27 Al–8 Cr	As-cast	Martensitic	α-Cr spheres	Mostly γ'	None	α-Cr needles
	850 °C aged	β	γ' lamellae	α-Cr	None	None
	1100 °C aged	β	γ' lamellae	Mostly γ'	α-Cr needles	None
Ni–20 Al–13 Co–9 Cr–4 Ti–1 Mo–1 V	As-cast	Martensitic	Negligible	Mostly γ'	Negligible	None
	850 °C aged	β	γ' and σ	γ/γ'	σ	None
	1100 °C aged	β	γ' and σ	γ/γ'	None	None

TABLE II Summary of compositional data (from SEM-based EDS analyses) obtained from the materials examined

Overall composition (at %)	Condition	Average composition (at %)	
		Dendritic region	Interdendritic region
Ni–25 Al–14 Cr	As-cast	Ni–32 Al–11 Cr	Ni–13 Al–31 Cr
	850 °C aged	Ni–35 Al–9 Cr	Ni–17 Al–40 Cr
	1100 °C aged	Ni–35 Al–5 Cr	Ni–13 Al–27 Cr
Ni–29 Al–22 Cr	As-cast	Ni–30 Al–12 Cr	Ni–12 Al–34 Cr
	850 °C aged	Ni–40 Al–3 Cr	Ni–13 Al–51 Cr
	1100 °C aged	Ni–35 Al–3 Cr	Ni–17 Al–22 Cr
Ni–27 Al–8 Cr	As-cast	Ni–32 Al–12 Cr	Ni–13 Al–31 Cr
	850 °C aged	Ni–31 Al–9 Cr	Ni–0 Al–97 Cr
	1100 °C aged	Ni–37 Al–2 Cr	Ni–20 Al–63 Cr
Ni–20 Al–13 Co–9 Cr–4 Ti–1 Mo–1 V	As-cast	Ni–30 Al–9 Co–6 Cr–2 Ti–0.5 Mo–1V	Ni–14 Al–16 Co–14 Cr–4 Ti–1 Mo–1V
	850 °C aged	Ni–22 Al–11 Co–10 Cr–4 Ti–1 Mo–1V	Ni–11 Al–16 Co–17 Cr–4 Ti–3 Mo–1V
	1100 °C aged	Ni–32 Al–10 Co–7 Cr–3 Ti–0 Mo–0.5V	Ni–13 Al–16 Co–14 Cr–4 Ti–2 Mo–1V

Note: the compositions given for the dendritic and interdendritic regions exclude α-Cr needles that cross dendrite boundaries.

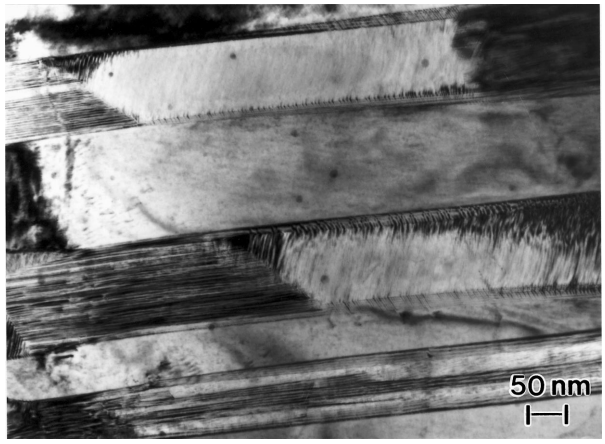

(a)

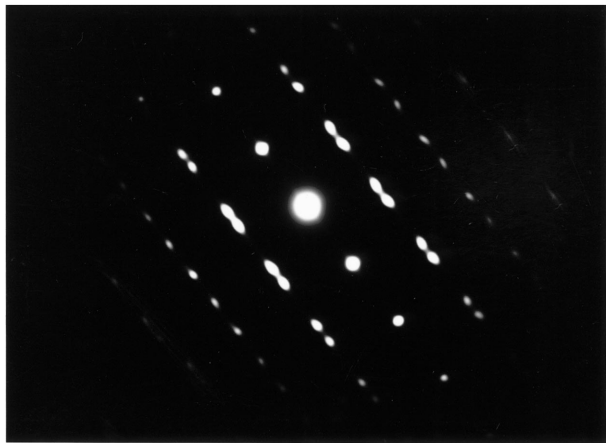

(b)

Figure 1 Intradendritic $L1_0$ martensite present in the as-cast condition: (a) BF micrograph (Ni–29 at % Al–22 at % Cr alloy); (b) NBD pattern with $\mathbf{B} = [1\,0\,1]_{L1_0}$ (Ni–25 at % Al–14 at % Cr alloy).

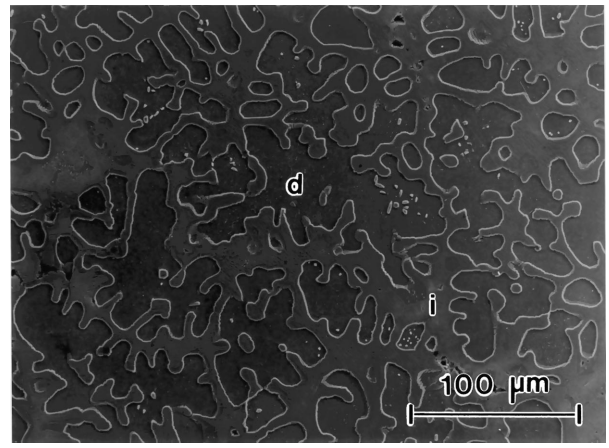

(a)

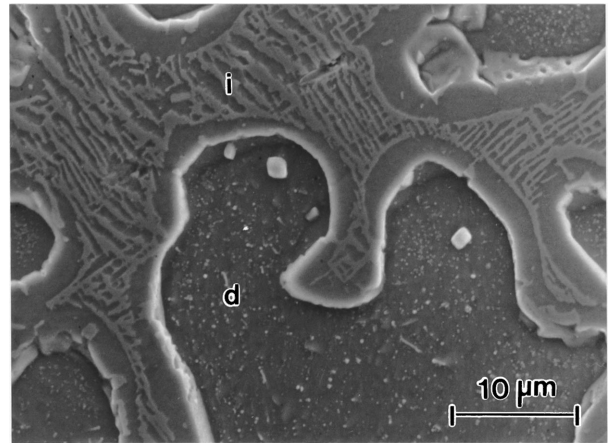

(b)

Figure 2 SEIs showing the microstructure of the Ni–20 at % Al–13 at % Co–9 at % Cr–4 at % Ti–1 at % Mo–1 at % V alloy aged for 140 h at 1100 °C (β-phase dendrites are labeled as "d" and the interdendritic γ/γ' region is denoted by "i"): (a) overall microstructure; (b) detailed microstructure.

3.1. Overview of microstructural and compositional features

All of the materials examined were found to solidify dendritically, with the dendrite matrices undergoing complete martensitic transformation during cooling. In the as-cast condition, nickel-rich dendrites with a twinned $L1_0$-type matrix were observed (Fig. 1) in all cases. No evidence was found of the formation of the 7R transitional phase [e.g., 13] or other β-phase decomposition products. Aging at both 850 and 1100 °C in general had the effect of transforming the dendrite interiors from $L1_0$ martensite to a range of β-γ' two-phase microstructures (an example of a β dendritic microstructure is shown in Fig. 2). The character of these β-γ' microstructures varied significantly between the different materials examined, and this is discussed in detail in section 3.2.

Chromium was found to have segregated to the interdendritic regions of the as-cast samples. Conversely, the dendrites of the three Ni–Al–Cr ternary alloys were found to be rich in aluminum when compared to the interdendritic regions. In the as-cast Ni–Al–Cr alloys, the compositions (Table II) of both the dendritic and interdendritic regions varied only slightly from alloy to alloy. This contrasts strongly with the significant difference in overall composition between the three alloys (overall aluminum contents range from 25 to 29 at % and chromium contents from 8 to 22 at %). Variations in the volume fraction occupied by the interdendritic regions accommodated the different overall compositions.

Chromium is a γ stabilizer, at the expense of both β and γ' [9]. However, with the exception of the 22 at % Cr alloy, the matrices of the interdendritic regions in the as-cast Ni–Al–Cr materials were found to consist largely of single-phase γ'. In the Ni–Al–Cr alloys, the failure to observe significant interdendritic γ-phase precipitation appeared to result from the extensive precipitation of α-Cr (A2-type chromium-based disordered solid solution). Precipitation of α-Cr that influenced the composition of the interdendritic matrix occurred both interdendritically and across dendrite boundaries. The formation of α-Cr removed γ-stabilizing chromium from solution in the interdendritic matrix. Precipitation of α-Cr is discussed in further detail in section 3.3.

In the case of the Ni–20 at % Al–13 at % Co–9 at % Cr–4 at % Ti–1 at % Mo–1 at % V alloy in the as-cast condition, segregation of cobalt, chromium, titanium, and molybdenum to the interdendritic regions was observed. Although the formation of α-Cr did not take place in the as-cast material, the interdendritic regions

were single-phase γ'. Jia *et al.* [9] give the following partition coefficients γ' and $\gamma(k^{\gamma'/\gamma})$ for a temperature of 1100 °C: chromium 0.79, cobalt 0.58, molybdenum 1.60, and titanium 1.82 (all data are for dilute alloys). Thus, although the interdendritic regions contained 16 at% of cobalt and 14 at% of chromium, γ-stabilization by these elements was presumably (at least in part) counteracted by the presence interdendritically of γ'-stabilizing titanium and molybdenum.

In some cases, aging at both 850 and 1100 °C had the effect of (at least partially) re-solutioning α-Cr and hence releasing γ-stabilizing chromium into the interdendritic matrix. This correlated to the formation of γ/γ' interdendritic microstructures in the as-aged condition. In the case, however, of the Ni–27 at% Al–8 at% Cr alloy aged at 850 °C, the interdendritic regions were largely consumed by growth of the dendrites and the residual interdendritic regions were composed entirely of α-Cr. Changes in the distribution of α-Cr precipitates, in particular, complicated the trend in overall dendritic and interdendritic composition with aging, and no single simple correlation between aging treatment and these compositions was apparent.

Based upon overall compositional and microstructural features discussed above, the development of specific phases will now be discussed in detail.

3.2. Intradendritic precipitation of γ'

As was noted above, aging of the as-cast materials at both 850 and 1100 °C resulted in transformation of the $L1_0$ martensite to the β-phase. After furnace cooling to room-temperature, β plus γ' two-phase microstructures were often observed in aged samples. The $L1_0$ martensite phase is fully reversible on re-heating (and this can be directly observed using hot-stage TEM [11]). Indeed, the existence of a fully reversible martensitic transformation forms the basis of the shape-memory effect observed in (nickel-rich) NiAl [8]. Thus, the $L1_0$ martensite must have first transformed back to the B2 type β-phase and only subsequently precipitated γ'. In these circumstances, the morphology of the $L1_0$ martensite could have no influence on the morphology of the γ' precipitates. Thus, "inheritance" of the morphology of the $L1_0$ martensite plates by lamellar γ' precipitates, as was proposed by Kainuma *et al.* [14] for γ' lamellae formed in an Ni–25 at% Al–15 at% Fe alloy, does not seem plausible [15]. This conclusion is of some importance in the present work as the matrix of the Ni–27 at% Al–8 at% Cr alloy was found (Fig. 3) to consist of a lamellar two-phase mixture of β and γ' (such that the γ' lamellae typically possessed a width of around 400–600 nm and were separated by β-phase regions possessing a width of around 200–400 nm).

The γ' lamellae were observed to form low-angle boundaries where adjacent γ' lamellae met (typically these were misoriented by around 1 to 2°). However, most interfaces were of the β-γ' type, rather than γ'-γ'. Furthermore, β-β interfaces were not generally observed within the lamellar β-γ' microstructure. The extent of intradendritic precipitation of the γ' and β-phases (in the 850 and 1100 °C aged Ni–27 at% Al–8 at% Cr alloy) was roughly similar and hence, at first sight, distinct designations of "matrix" and "second phase" might appear misleading. However, on further investigation, it was noted that the β-phase (Fig. 3c) formed a continuum within a given dendrite, which was not the case for the γ', which was composed of discrete, slightly mutually misoriented lamellae. Hence, the intradendritic microstructure of the 850 and 1100 °C aged Ni–27 at% Al–8 at% Cr alloy is best described as a γ' second phase in a β-phase matrix. This is consistent with the precipitation of γ' from nickel-rich β (present after reversion of the $L1_0$ martensite to its β parent phase).

A noticeable feature of the γ' lamellae in the Ni–27 at% Al–8 at% Cr alloy was the absence of twinning. Given that the $L1_0$ martensite plates in the as-cast material were extensively twinned, this provides a further argument against inheritance of the morphology of the $L1_0$ martensite by the γ' lamellae.

In contrast to the lamellar mode of γ' precipitation found in the Ni–27 at% Al–8 at% Cr alloy, formation of roughly ellipsoidal γ' precipitates in a β-phase matrix was observed after 850 and/or 1100 °C aging of the other three materials investigated. The γ' precipitates varied somewhat in size from material to material. Precipitate dimensions also depended upon the heat-treatment temperature employed and the position of the host dendrite in the arc-melted buttons. However, a precipitate length of around 500 nm–1 μm and width of around 200–600 nm was "typical". In general, the ellipsoidal precipitates were twinned (Fig. 4). Often, but not invariably, a single midrib twin boundary was observed.

The precipitation of (γ and/or) γ' from nickel-rich β can occur [15] with both Nishiyama–Wassermann and Kurdjumov–Sachs-type orientation relationships, such that:

$$[0\,0\,1]_\beta \;//\; [1\,1\,0]_{\gamma'}$$
$$(1\,1\,0)_\beta \;//\; (1\,\bar{1}\,1)_{\gamma'}$$

for the Nishiyama–Wassermann orientation relationship and

$$[1\,1\,1]_\beta \;//\; [1\,1\,0]_{\gamma'}$$
$$(\bar{1}\,1\,0)_\beta \;//\; (1\,\bar{1}\,\bar{1})_{\gamma'}$$

for the Kurdjumov–Sachs orientation relationship. In the present investigation, both of these orientation relationships were observed (some examples are shown in Figs 4c and 5) within any given sample. However, within a particular dendrite, only one of the two orientation relationships was usually encountered (although this was not always the case). Given that the misorientation between the Nishiyama–Wassermann and Kurdjumov–Sachs-type orientation relationships involves only a small rotation, the co-existence of these two orientation relationships is not unreasonable.

Yang *et al.* [16] have proposed a model for the precipitation of midrib twinned γ' from nickel-rich β. In Yang *et al.*'s model, γ' nucleates on the domain boundaries of ordered domains of antisite defects. The twin boundary

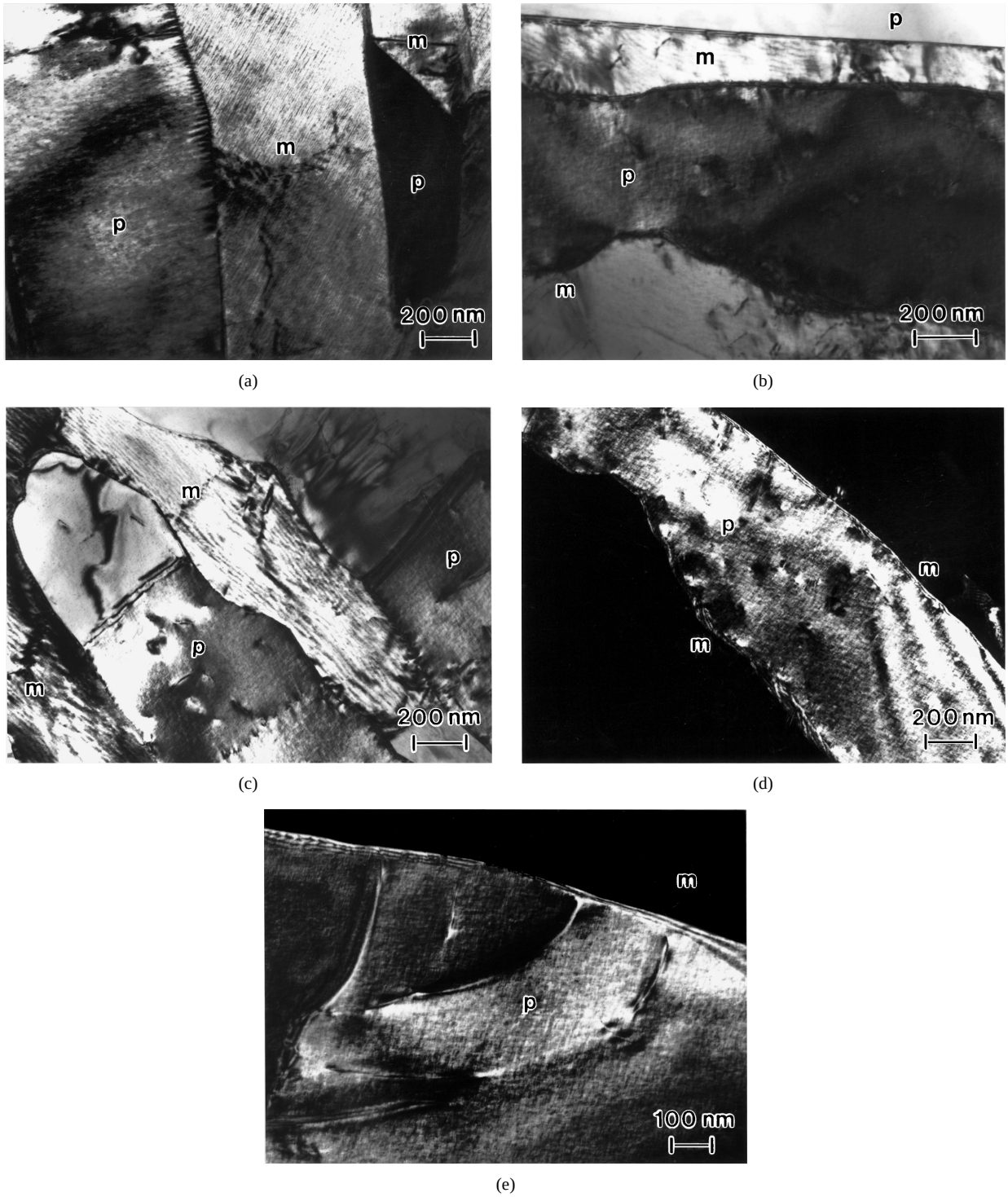

Figure 3 Formation of intradendritic γ' lamellae in the Ni–27 at % Al–8 at % Cr alloy aged for 140 h at 850 °C ($m = \beta$-phase matrix and $p = \gamma'$ precipitates): (a–c) BF micrographs; (d–e) DF images with $\mathbf{g} = (200)_{\gamma'}$.

then corresponds to the plane of the antisite domain boundary and the twinning results from the growth of γ' with different variants of the Nishiyama–Wassermann orientation relationship (in Yang *et al.*'s case) into the β-phase.

While the formation of antisite defects is well documented in nickel-rich B2 NiAl (for which the antisite defects consist of nickel atoms on aluminum sites [17]), no evidence has been found in the literature for the ordering of these defects into distinct domains. Furthermore, in the present case, twinning was observed even when the γ' precipitates nucleated on other (previously formed) γ' precipitates. In such a case, unless uncleation occurred on γ' precipitate–antisite domain boundary junctions (which would presumably be relatively infrequent unless the antisite domain size were small) an alternative mechanism would be required. One conceivable possibility is that the twinning results from an attempt to accommodate this misfit between the β and γ' phases. However, further investigation of this suggestion is required.

In (qualitative) TEM–EDS investigations the intradendritic γ'-phase was found, as would be expected, to be lower in aluminum than the adjacent β-phase. The

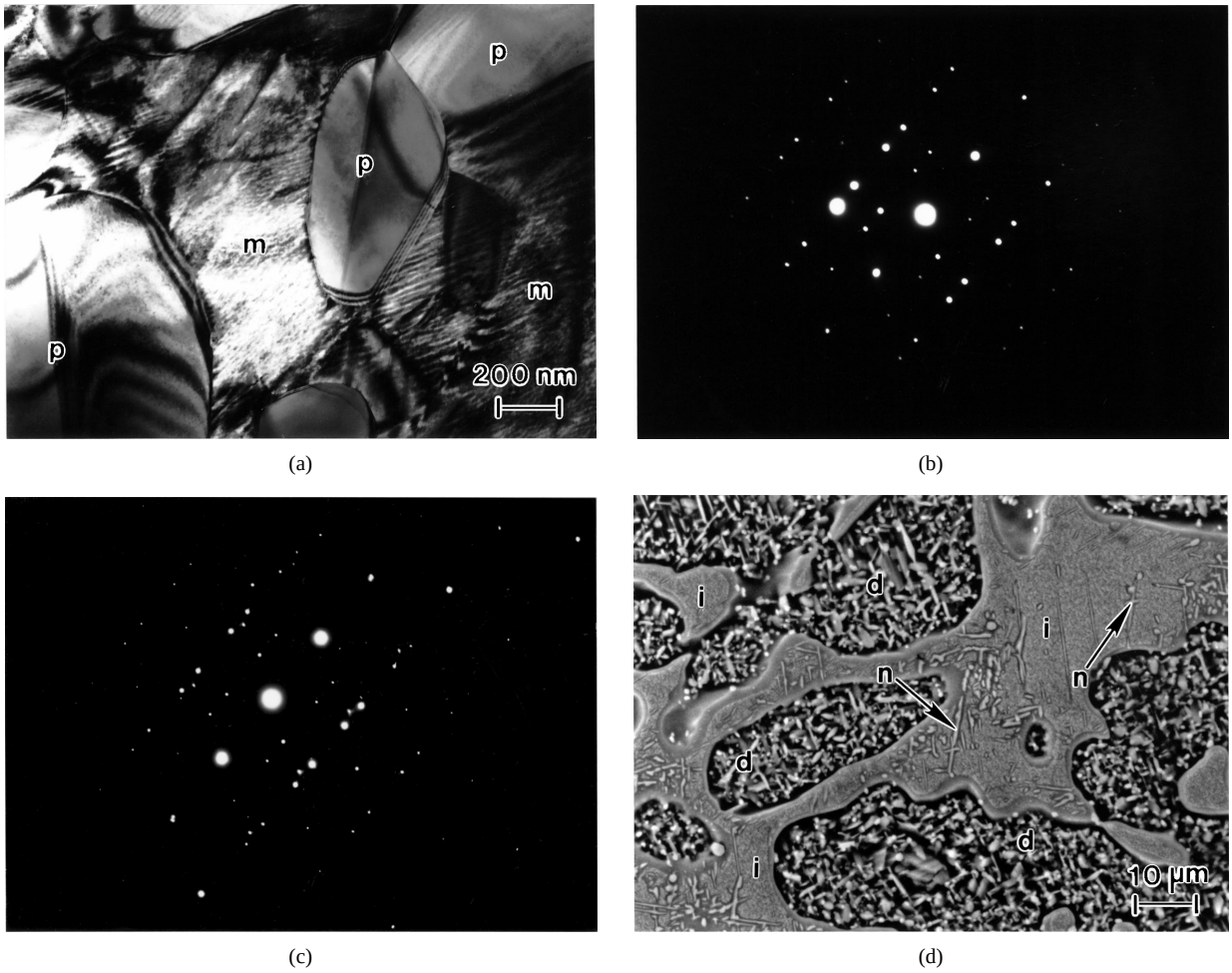

Figure 4 Twinned γ' precipitated within the β-phase dendrite matrix of the Ni–24 at % Al–11 at % Co–9 at % Cr–4 at % Ti–1 at % Mo–1 at % V alloy aged for 140 h at 850 °C ($m = \beta$-phase, $p = \gamma'$ precipitates, $d = \beta$-phase dendrites with intradendritic γ' precipitates, i = interdendritic γ/γ' and $n = \sigma$-phase interdendritic needles): (a) BF micrograph; (b) SAD with $\mathbf{B} = [1\,1\,0]_{\gamma'}$; (c) SAD with $\mathbf{B} = [1\,1\,0]_{\gamma'}$ // $[1\,1\,1]_{\beta}$ showing a Kurdjumov–Sachs-type orientation relationship; and (d) SEI showing the extensive intradendritic precipitation of γ'. Note also the existence of an interdendritic γ/γ' matrix with σ-phase needles.

chromium content of the intradendritic β and γ' phases in the three Ni–Al–Cr alloys was (in general) roughly similar, which is to be expected, given that the partition co-efficient between γ' and β ($k^{\gamma'/\beta}$) is approximately unity for chromium [9]. However, an anomaly was observed in the Ni–20 at % Al–13 at % Co–9 at % Cr–4 at % Ti–1 at % Mo–1 at % V alloy aged at 850 °C, for which chromium generally partitioned to the β-phase. The origin of this anomalous behaviour is not known at this time. The value of $k^{\gamma'/\beta}$ for cobalt is similar to that for chromium and, in the Ni–20 at % Al–13 at % Co–9 at % Cr–4 at % Ti–1 at % Mo–1 at % V alloy, these two elements behaved similarly, showing no marked preference for either the β or the γ' phase in the 1100 °C aged condition. In contrast, titanium was found to segregate to the γ' phase and this correlates with a $k^{\gamma'/\beta}$ value of 4.06 [9]. The average intradendritic molybdenum and vanadium contents of the Ni–20 at % Al–13 at % Co–9 at % Cr–4 at % Ti–1 at % Mo–1 at % V alloy were at, or below, 1 at % and thus were close to the detection limit for EDS. Hence, it was not possible to make a convincing determination of the segregation behavior of these two elements.

In Table I, it is noted that, although aging at 850 and 1100 °C usually resulted in the formation of intradendritic γ', γ'-free dendrites were observed for the Ni–25 at % Al–14 at % Cr alloy aged at 850 °C. A further anomaly was also observed in the Ni–29 at % Al–22 at % Cr alloy aged at 850 and 1100 °C. In this sample, some regions of the dendrites retained some $L1_0$ martensite (Fig. 6), whereas adjacent regions of the same dendrites were transformed to a β-matrix with ellipsoidal twinned γ' precipitates.

3.3. Formation of α-Cr

The precipitation of both intradendritic and interdendritic α-Cr was observed in many of the materials examined. In addition, large α-Cr needles were often observed to cross over dendrite boundaries, and hence these needles could not be described uniquely as either intradendritic or interdendritic precipitates. In all cases, the α-Cr precipitates were aluminum-free (within the detection capability of EDS). However, some of the α-Cr contained up to 5 at % Ni.

In the as-cast condition, intradendritic α-Cr formed as spheroidal precipitates (Fig. 7). Field *et al.* [18] observed that α-Cr precipitated in the β-phase is only semi-coherent and forms distinctive interfacial dislocation networks. In the present investigation, in cases

(a)

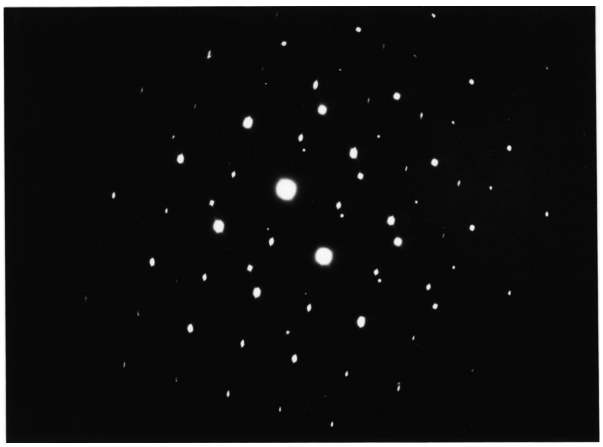

(b)

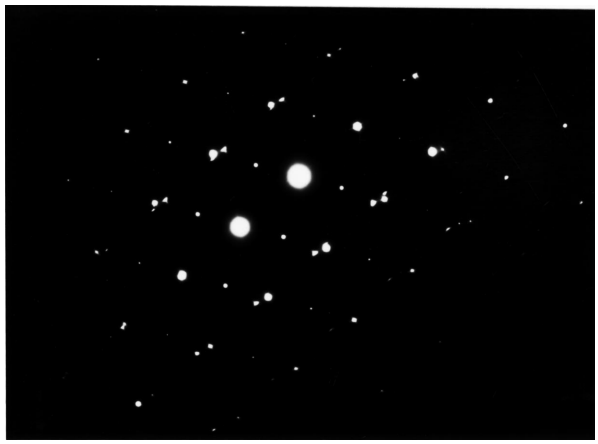

(c)

Figure 5 SAD patterns showing γ' precipitated within the β-phase dendrite matrix of Ni–Al–Cr samples aged for 140 h at 1150 °C: (a) $\mathbf{B} = [1\,1\,0]_{\gamma'}$ (Ni–29 at % Al–22 at % Cr alloy); (b) $\mathbf{B} = [1\,1\,0]_{\gamma'}$ // $[0\,0\,1]_{\beta}$ showing a Nishiyama–Wassermann-type orientation relationship (Ni–27 at % Al–8 at % Cr alloy); (c) $\mathbf{B} = [1\,1\,0]_{\gamma'}$ // $[1\,1\,1]_{\beta}$ showing a Kurdjumov–Sachs-type orientation relationship (Ni–27 at % Al–8 at % Cr alloy).

(a)

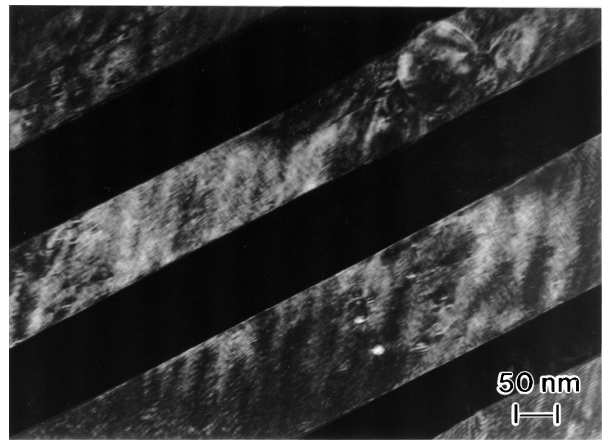

(b)

Figure 6 $L1_0$ martensite observed intradendritically in the Ni–29 at % Al–22 at % Cr alloy aged for 140 h at 1100 °C: (a) BF micrograph. Note the presence of α-Cr second-phase precipitates (labeled as "s")—these precipitates were not present in the non-martensitic regions of the dendrites; (b) DF image with $\mathbf{g} = (\bar{1}\,\bar{1}\,\bar{1})_{L1_0}$.

where the α-Cr precipitates were relatively small (e.g., less than about 50 nm in diameter), coherent (elastically strained) interfaces were formed with the surrounding matrix. In contrast, larger (e.g., 100 nm diameter or larger precipitates) were semicoherent.

In the case of intradendritic α-Cr found in the as-cast materials (i.e., for the case of all three Ni–Al–Cr ternary alloys), the α-Cr precipitates were found to adopt the following orientation relationship to the surrounding $L1_0$ martensite (Fig. 7b):

$$[1\,0\,1]_{L1_0} \;//\; [1\,1\,1]_{\alpha\text{-Cr}}$$
$$(1\,1\,\bar{1})_{L1_0} \;//\; (\bar{1}\,1\,0)_{\alpha\text{-Cr}}$$

The morphology of the α-Cr precipitates appeared completely independent of that of the $L1_0$ martensite. Thus, it might be the case that the α-Cr nucleated from the β-phase and that the latter only subsequently underwent martensitic transformation. In such a case, the observed orientation relationship between the martensite and the α-Cr would be that between the β-phase parent and $L1_0$ type product of the martensitic transformation. The observed (Kurdjumov–Sachs type) orientation relationship is compatible with (but does not of course directly support) this suggestion. Aging of the Ni–Al–Cr alloys generally led to dissolution of the intradendritic α-Cr. This was unexpected as, once formed, α-Cr is generally stable in similar systems [19].

The formation of α-Cr precipitates residing entirely in the interdendritic region took on two forms. The first of these, as observed in the Ni–27 at % Al–8 at % Cr alloy arose when significant growth of the β-phase occurred during 850 °C aging, to the point where only occasional isolated interdendritic regions remained.

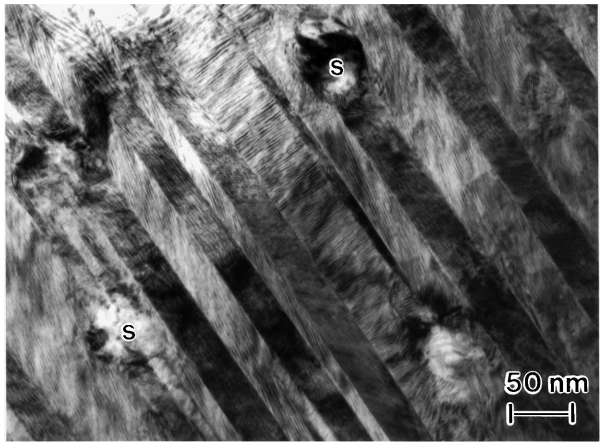

(a)

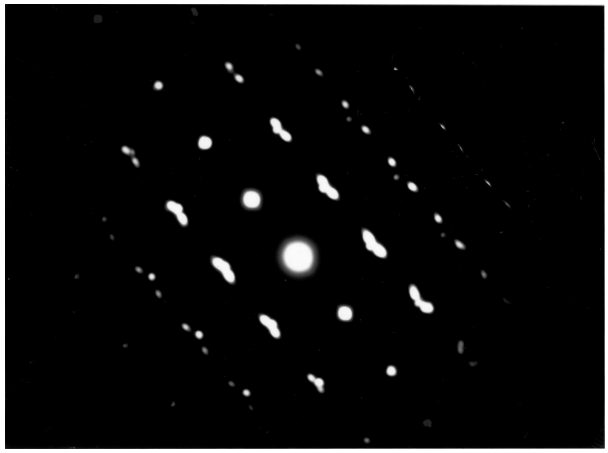

(b)

Figure 7 Precipitation of spheroidal α-Cr in as-cast Ni–Al–Cr samples: (a) BF micrograph showing the $L1_0$ martensite dendrite matrix of the Ni–29 at % Al–22 at % Cr alloy and α-Cr second-phase precipitates (labeled as "s"); (b) NBD pattern with $\mathbf{B} = [1\,0\,1]_{L1_0}$ // $[1\,1\,1]_{\alpha\text{-Cr}}$ showing a Kurdjumov–Sachs-type orientation relationship between α-Cr precipitates and the $L1_0$ martensite in the Ni–25 at % Al–14 at % Cr material.

Given the low solubility of chromium in the β-phase (around 4 at % for stoichiometric NiAl at 850 °C [20]), the growing β-phase rejected chromium back into the remaining interdendritic regions during aging (thus continuing in the solid-state the chromium redistribution observed after solidification). This chromium rejection correlated, in the Ni–27 at % Al–8 at % Cr alloy, with the transformation of the residual interdendritic regions to single-phase α-Cr. Within any given region of a sample, the single-phase α-Cr was of a constant crystallographic orientation. However, no orientation relationship was noted with the adjacent dendrites.

The second type of interdendritic α-Cr precipitates observed in the present work were needles, typically with a length of around 5 μm and a width of about 2 μm. These needles were formed either in the as-cast condition (Ni–25 at % Al–14 at % Cr alloy) or after aging (Ni–29 at % Al–22 at % Cr aged at 850 °C or Ni–27 at % Al–8 at % Cr aged at 1100 °C). These fine needles possessed a Nishiyama–Wassermann-type orientation relationship to the surrounding (γ'-phase) interdendritic matrix.

In addition to the relatively fine α-Cr needles, coarse α-Cr needles (typically in the range of 50 to 200 μm long and around 5 to 10 μm wide) were observed. These coarse α-Cr needles (Fig. 8) frequently crossed dendrite boundaries and the position of the needles appeared to be little influenced by the local topographic orientation of the dendrite boundaries. Unique orientation relationships could not be identified between the α-Cr needles and other phases present in the samples. However, given the large size of the coarse α-Cr needles, problems with differential thinning were experienced during ion milling. Differential thinning impeded the identification of any orientation relationships that may have been present. The detailed mechanisms leading to the formation of both the fine and coarse α-Cr needles remain unclear.

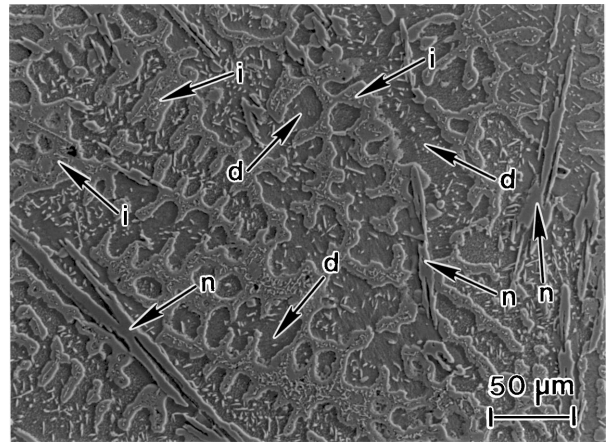

Figure 8 SEI illustrating the overall microstructure of the Ni–25 at % Al–14 at % Cr alloy aged for 140 h at 850 °C. Note the presence of large α-Cr needles (labeled as "n") crossing dendrite boundaries (β-phase dendrites with intradendritic α-Cr precipitates are labeled as "d," while the interdendritic regions consisting of a γ/γ' matrix and α-Cr precipitates are denoted by "i").

3.4. The generation of interdendritic γ' and γ/γ' microstructures

As was noted in section 3.1 above, the interdendritic matrix of all but one of the materials examined in the present work consisted, in the as-cast condition, of almost single-phase γ' (only occasional regions of γ were observed). The sole exception to this trend was the Ni–29 at % Al–22 at % Cr alloy. In this material, dendrite boundaries were coated with a layer of single-phase γ' with a thickness typically in the range of 200–500 nm. This layer of single-phase γ', which contained numerous antiphase boundaries, was cube-cube orientation-related to the interdendritic matrix. However, the γ' layer was not orientation-related to the dendrites (an orientation relationship was not observed between the dendritic and interdendritic matrices). The remainder of the interdendritic region was composed of γ' cuboids whose edges possessed lengths of around 100–200 nm. These γ' precipitates were cube-cube orientation-related to the γ-phase interdendritic matrix.

The formation of γ/γ' microstructures (an example of which is given in Fig. 2b) during aging at either 850 or 1100 °C was found to require complete dissolution of the α-Cr precipitates contained within, or intersecting, the interdendritic regions. In contrast, in

cases where existing α-Cr remained present, or where new α-Cr formed during aging, insufficient chromium remained in solution in the interdendritic matrix to stabilize the γ-phase. In these circumstances, a single-phase γ' matrix resulted, even when (in the case of the Ni–29 at % Al–22 at % Cr alloy) the interdendritic matrix consisted of two-phase γ/γ' in the as-cast condition. When γ/γ' microstructures did form during aging, the interdendritic regions closely resembled those found in the as-cast Ni–29 at % Al–22 at % Cr material.

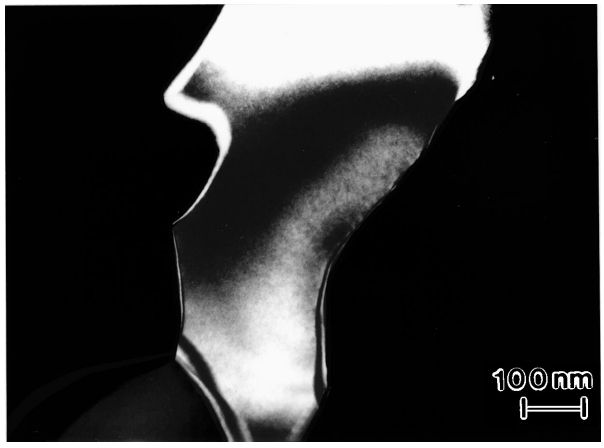

(a)

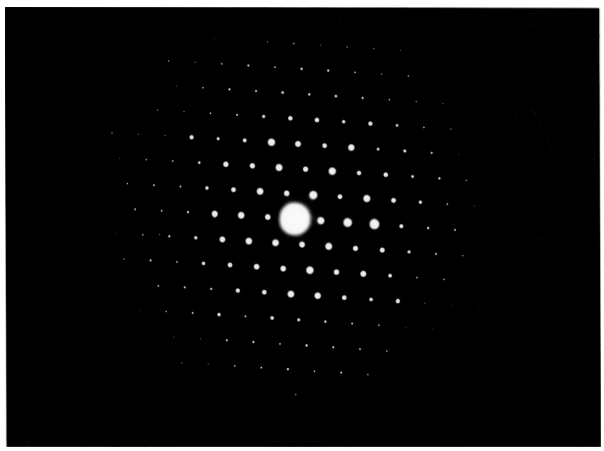

(b)

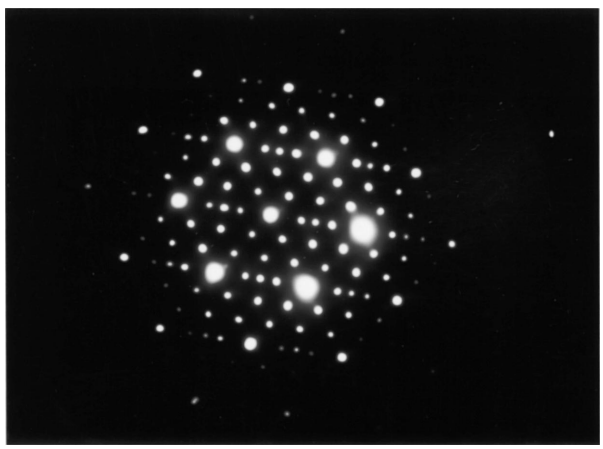

(c)

Figure 9 Precipitation of $M_{23}X_6$ in Ni–Al–Cr materials arc-melted with a graphitic electrode: (a) DF image employing $g = (\bar{2}\,2\,2)_{M_{23}X_6}$ showing an $M_{23}X_6$ precipitate in the Ni–25 at % Al–14 at % Cr alloy aged for 140 h at 1100 °C; (b) SAD pattern produced with $\mathbf{B} = [1\,1\,0]_{M_{23}X_6}$ (Ni–27 at % Al–8 at % Cr alloy aged for 140 h at 850 °C); (c) SAD pattern corresponding to $\mathbf{B} = [1\,1\,0]_{M_{23}X_6/\gamma'}$ showing the cube-cube orientation relationship of an $M_{23}X_6$ carbide and the γ' interdendritic matrix of the Ni–27 at % Al–8 at % Cr alloy aged for 140 h at 850 °C.

3.5. Other phases

All of the materials investigated in the present work were arc-melted. When a graphitic electrode was employed, occasional $M_{23}X_6$ (for which M was chromium and X carbon) carbides were observed (Fig. 9) interdendritically with a cube-cube orientation relationship to the interdendritic (γ/γ' or γ') matrix. These carbides presumably formed as a result of carbon incorporation into the melt from the electrode and subsequent reaction with chromium. Likewise, the use of a tungsten electrode correlated with the presence of a few randomly oriented metallic tungsten particles.

In contrast to the $M_{23}X_6$ precipitates and tungsten particles resulting from the arc-melting process, the precipitation (Fig. 10) of σ-phase (rich in chromium, molybdenum, and cobalt) was an intrinsic characteristic of the Ni–20 at % Al–13 at % Co–9 at % Cr–4 at % Ti–1 at % Mo–1 at % V alloy. A small amount of intra- and interdendritic σ was observed in this material after aging at 850 °C, whereas aging at 1100 °C led only to

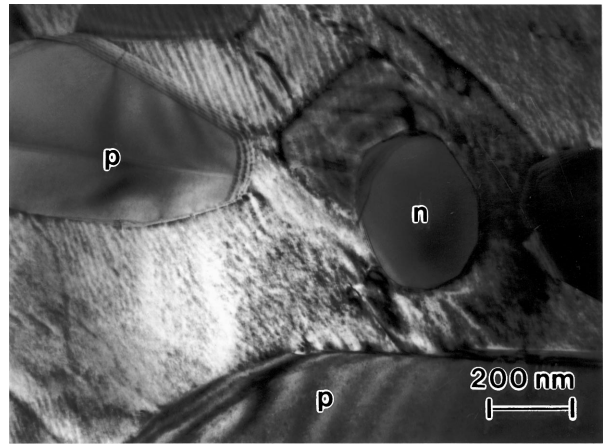

(a)

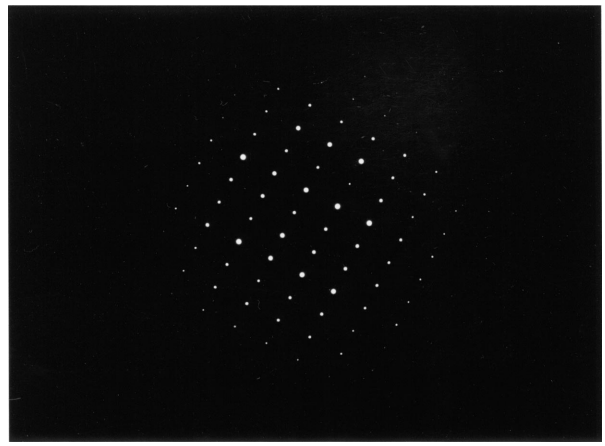

(b)

Figure 10 Intradendritic precipitation of γ' (labeled as "p") and σ-phase (labeled as "n") in the Ni–20 at % Al–13 at % Co–9 at % Cr–4 at % Ti–1 at % Mo–1 at % V alloy aged for 140 h at 850 °C: (a) BF micrograph (note the change of orientation of this figure with respect to Fig. 4a). (b) SAD pattern ($\mathbf{B} = [1\,1\,0]_{\sigma}$).

the formation of occasional intradendritic σ-phase precipitates. In the carbon-rich material from which the Ni–20 at % Al–13 at % Co–9 at % Cr–4 at % Ti–1 at % Mo–1 at % V alloy was derived, extensive precipitation of interdendritic $M_{23}X_6$ was observed. In contrast, in the present work on tungsten-electrode arc-melted material for which no intentional addition of carbon was made, only a small amount of σ was formed.

4. Conclusions

In this paper, a study of microstructural development in the following materials has been presented: Ni–25 at % Al–14 at % Cr, Ni–29 at % Al–22 at % Cr, Ni–27 at % Al–8 at % Cr and Ni–20 at % Al–13 at % Co–9 at % Cr–4 at % Ti–1 at % Mo–1 at % V. These alloys have been investigated both in the as-cast condition and after 140 h duration aging treatments conducted at both 850 and 1100 °C. As a result of this work, the following conclusions were drawn:

- All of the materials investigated underwent martensitic transformation of the B2-type β-phase formed during solidification. Hence, in the as-cast condition, all of the materials investigated had dendrite matrices composed of $L1_0$ martensite.
- Aging of the as-cast material at either 850 or 1100 °C for 140 h was (in general) sufficient to cause complete reversal of the $L1_0$ martensite to the β-phase and subsequent precipitation of intradendritic γ'. In any given material and condition, both Nishiyama–Wassermann and Kurdjumov–Sachs-type orientation relationships could be observed between the β and γ' phases. Marked disparities were noted in γ' morphology between the different materials examined.
- Three distinct classes of α-Cr precipitation were noted in the materials examined. These classes were as follows:

  1) Intragranular α-Cr precipitates in the as-cast materials formed with a Kurdjumov–Sachs-type orientation relationship to the $L1_0$ martensite dendrite matrices. Those α-Cr precipitates remaining after aging (and any fresh intradendritic α-Cr formed during aging) were cube-cube orientation-related to the β-phase.

  2) Interdendritic α-Cr precipitated with a Nishiyama–Wassermann-type orientation relationship to the surrounding γ'-phase.

  3) Coarse needles of α-Cr were observed to cross dendrite boundaries.
- In the as-cast condition, the extensive precipitation of α-Cr removed γ-stabilizing chromium from solution in the interdendritic matrix, resulting in the formation of single-phase interdendritic γ' in the three Ni–Al–Cr alloys examined. Re-solutioning of α-Cr impinging upon and/or contained within the interdendritic regions was necessary to allow the formation of interdendritic γ/γ' during aging at 850 or 1100 °C.

Acknowledgments

The research described in this paper was supported by the NSF EPSCoR program. Funding for instrumentation was provided by the NSF ARI program.

References

1. P. S. KHADKIKAR, K. VEDULA and B. S. SHABEL, *MRS Symp. Proc.* **81** (1987) 157.
2. S. GUHA, P. R. MUNROE and I. BAKER, *ibid.* **133** (1989) 633.
3. K. ISHIDA, R. KAINUMA, N. UENO and T. NISHIZAWA, *Metall. Trans. A* **22A** (1991) 441.
4. R. D. FIELD, D. D. KRUEGER and S. C. HUANG, *MRS Symp. Proc.* **133** (1989) 567.
5. M. LARSEN, A. MISRA, S. HARTFIELD-WUNSCH, R. D. NOEBE and R. GIBALA, *ibid.* **194** (1990) 191.
6. A. MISRA, R. D. NOEBE and R. GIBALA, *ibid.* **273** (1992) 205.
7. *Idem., ibid.* **288** (1993) 483.
8. K. ENAMI and S. NENNO, *Metall. Trans. A* **2** (1971) 1487.
9. C. C. JIA, K. ISHIDA and T. NISHIZAWA, *Metall. Mater. Trans. A* **25A** (1994) 473.
10. W. F. GALE and R. V. NEMANI, *Mater. Sci. Engng.* **A192/193** (1995) 868.
11. W. F. GALE, R. V. NEMANI and J. A. HORTON, *J. Mater. Sci.* **31** (1995) 1681.
12. W. F. GALE, T. C. TOTEMEIER and J. E. KING, *Microstructural Sci.* **21** (1994) 61.
13. A. G. KHACHATURYAN, S. M. SHAPIRO and S. SEMENOVSKAYA, *Phys. Rev. B* **43** (1991) 10-832.
14. R. KAINUMA, S. IMANO, H. OHTANI and K. ISHIDA, *Intermetallics* **4** (1996) 37.
15. W. F. GALE, *ibid.* **4** (1996) 585.
16. R. YANG, J. A. LEAKE and R. W. CAHN, *J. Mater. Res.* **6** (1991) 343.
17. P. GEORGOPOULOS and J. B. COHEN, *Scripta Metall.* **11** (1977) 147.
18. R. D. FIELD, D. F. LAHRMAN and R. DAROLIA, *Acta Metall. Mater.* **39** (1991) 2961.
19. W. F. GALE and J. E. KING, *J. Mater. Sci.* **28** (1993) 4347.
20. G. PETZOW and G. EFFENBERG (eds), "Ternary Alloys, A Comprehensive Compendium of Evaluated Constitutional Data and Phase Diagrams" (VCH Publishing, New York, 1991).

Received 21 November 1996
and accepted 6 August 1998